Measuring Code-Phase Differences due to Inter-Satellite Hardware Differences

Gabriel Wong, Yu-Hsuan Chen, R. Eric Phelts, Todd Walter, Per Enge,
Stanford University

BIOGRAPHY

Gabriel Wong is an Electrical Engineering Ph.D. candidate at the Stanford University GNSS Research Laboratory. He has previously received an M.S.(EE) from Stanford University, and a B.S.(EECS) from UC Berkeley. His current research involves signal deformation monitoring and mitigation for GNSS signals.

Yu-Hsuan Chen is a Post Doc in GPS Lab at Stanford University. He received his Ph. D in electrical engineering from National Cheng Kung University in Taiwan. His research interests include real-time GNSS software receiver and antenna array processing

R. Eric Phelts, Ph.D., is a research engineer in the Department of Aeronautics and Astronautics at Stanford University. He received his B.S. in Mechanical Engineering from Georgia Institute of Technology in 1995, and his M.S. and Ph.D. in Mechanical Engineering from Stanford University in 1997 and 2001, respectively. His research involves signal deformation monitoring techniques and analysis for SBAS, GBAS, and the GPS Evolutionary Architecture Study (GEAS).

Todd Walter, Ph.D., is a senior research engineer in the Department of Aeronautics and Astronautics at Stanford University. Dr. Walter received his Ph.D. from Stanford and is currently working on modernization of the Wide Area Augmentation System (WAAS) and defining future architectures to provide aircraft guidance. Key contributions include early prototype development proving the feasibility of WAAS, significant contribution to the WAAS MOPS, design of ionospheric algorithms for WAAS, and development of dual frequency algorithms for SBAS. He is a fellow of the Institute of Navigation and serves as its president.

Per Enge, Ph.D., is a professor of aeronautics and astronautics at Stanford University, where he is the Kleiner-Perkins Professor in the School of Engineering. He directs the GNSS Research Laboratory, which develops satellite navigation systems. He has been involved in the development of the Federal Aviation Administration's GPS Wide Area Augmentation System (WAAS) and Local Area Augmentation System (LAAS). For this work, Enge has received the Kepler, Thurlow, and Burka awards from the Institute of Navigation (ION). He received his Ph.D. from the University of Illinois. He is a member of the National Academy of Engineering and a Fellow of the IEEE and the ION.

ABSTRACT

This paper focuses on the hardware demonstration of pseudorange domain errors from nominal signal deformation, as seen at the output of actual hardware receivers. To see these errors in the current single-frequency configuration, the following procedural steps were necessary to highlight the error contributions:

- Careful siting of antenna to reduce multipath — as it is the other correlator spacing-dependent error source
- Multiple "receivers" with wide front-end bandwidths and with the flexibility of implementing both narrow and wide correlator discriminators for tracking
- A known, zero-baseline differential receiver configuration with common clock to remove all other common mode errors

With these steps, the effects of nominal signal deformation on pseudorange domain performance are clearly and directly seen for the first time, verifying past results.

The proposed method avoids specialized hardware such as large dish antennas; instead, widely-available COTS hardware and a more easily-accessible dish antenna are used. This provides a practical and convenient means of monitoring signal deformations and for testing and verifying various mitigation strategies. Furthermore, this method is easily adapted to upcoming multi-constellation, multi-frequency systems.

INTRODUCTION

Signal deformations are deviations of GNSS satellite signals from ideal and originate from the satellite's signal generation hardware chain. Under nominal, everyday operating conditions, there are nominal signal deformations that are different for individual satellites [9], as shown in Fig 1.
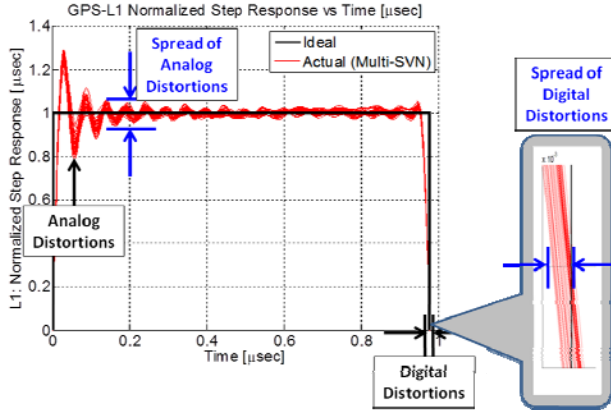

Figure 1. Nominal *Analog and Digital Distortions as measured for different GPS satellites. Data collected with SRI 46m-Dish: Aug 2008, Jul 2009, Aug 2010.*

When these broadcast GPS satellite signals are received by GPS receivers with different configurations – such as different filter bandwidths or correlator spacings in the tracking loops – range biases of 0.15m-0.3m are induced (see Fig 2). These in turn cause pseudorange and position errors [10, 11].
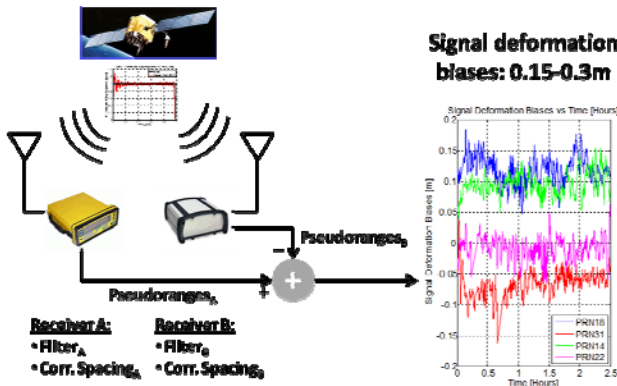

Figure 2. *Nominal signal deformations cause GPS receivers with different configurations (filter bandwidths and/ or correlator spacings in tracking loop) to experience differential range biases, pseudorange and position errors.*

For single frequency SBAS, the error bound for the ionosphere is dominant; the assumed error bound for signal deformation is small and insignificant in comparison (Fig **3**) **[2].**
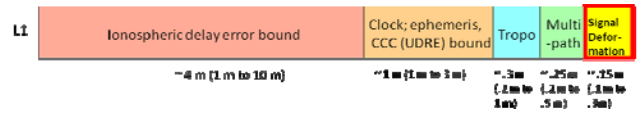

Figure 3. *Nominal Signal Deformation Error Bound is a small and rather insignificant component of the overall Single-Frequency SBAS Error Bound.*

In the case of dual-frequency or multi-frequency augmentation systems for aviation, measurements are scaled and combined to remove ionospheric errors. While this has the beneficial effect of lowering the overall error bound (sans ionospheric error bound), the scaling also amplifies the signal deformation error, which in turn requires a larger error bound (Fig **4**) **[2]**. This larger error bound for signal deformation then becomes a more significant component of the smaller, new overall error bound. Thus, nominal signal deformations may have an increased adverse impact/threat on the accuracy, integrity and availability of these systems.
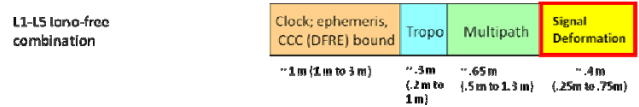

Figure 4. *In Dual-Frequency SBAS, the error bound for Nominal Signal Deformation is a more significant component of the smaller, new overall error bound. This is due to the scaling to remove ionospheric error and the removal of ionospheric error bounds.*

The situation is likely to be exacerbated with different deformations in multi-constellation systems. This accentuates the need for effective monitoring and mitigation strategies.

SIGNAL DEFORMATION – MATHEMATICAL DESCRIPTION

The following equations describe mathematically the signal deformation errors in the receiver.

Equation (1) shows the pseudorange equation for a single satellite in a single receiver configuration:

$$\rho = r + c[\delta t_u - \delta t^s] + I_p + T_p + \varepsilon_p + MP_p + SDM_p \quad\text{-----------------}(1)$$

where
ρ: pseudorange
r: true range
c: speed of light
δt_u: receiver clock error
δt^s: satellite clock error
I_p: Ionospheric error
T_p: Tropospheric error
ε_p: White noise at receiver
MP_p: Multipath error at receiver
SDM_p: Signal deformation error at receiver

Equation (2) shows the pseudorange observable for a single satellite, zero-baseline, differential receiver configuration. For this configuration, the reference receiver's (subscript n) tracking loop correlator spacing is at 0.1 chips, and user receiver's (subscript m) tracking loop correlator spacing is at 0.2 chips.

$$\rho_{m,n} = c\underbrace{[\delta t_{u,m} - \delta t_{u,n}]}_{\substack{\text{Clock bias: Eliminate} \\ \text{with common clock}}} + \varepsilon_{p,m} - \varepsilon_{p,n} + \underbrace{(MP_{p,m} - MP_{p,n})}_{\substack{\text{Multipath:} \\ \text{Time-varying;} \\ \text{possibly non-zero bias}}} + \underbrace{(SDM_{p,m} - SDM_{p,n})}_{\substack{\text{Signal Deformation:} \\ \text{Generally constant}}} \quad \text{-- (2)}$$

where
ρ: pseudorange
c: speed of light
$\delta t_{u,m}$: user receiver clock error
$\delta t_{u,n}$: reference receiver clock error
$\varepsilon_{p,m}$: White noise at user receiver
$\varepsilon_{p,n}$: White noise at reference receiver
$MP_{p,m}$: Multipath error at user receiver
$MP_{p,n}$: Multipath error at reference receiver
$SDM_{p,m}$: Signal deformation error at user receiver
$SDM_{p,n}$: Signal deformation error at reference receiver

Note that the only remaining errors are the differential receiver clock bias, which can be eliminated using a common clock, differential receiver white noise (which can be effectively removed by averaging) and the differential multipath and signal deformation errors.

Both differential multipath and signal deformation errors are dependent on filter bandwidths and group delays and also on the tracking loop correlator spacings. Signal deformation errors tend to be constant, while multipath errors are time-varying in general and may have non-zero biases, which may corrupt measurements of signal deformation biases. Thus, effective attenuation of multipath is imperative for accurate measurement of signal deformation errors.

The following summarizes what is required for accurate signal deformation error measurements:
- Low multipath antenna and environment
- Receivers with multiple correlator spacings in the tracking loop
- Common clock to synchronize the differential receivers

PAST MEASUREMENT WORK

Previous work to measure nominal signal deformation errors include:

- High gain (low noise), sequential, short data sets:
24-hour data collection campaign at the Stanford Research Institute (SRI) 46m, high-gain dish using a high-bandwidth, low noise data logger.

   Data sets were collected for the entire constellation of GPS satellites, one satellite at a time. Each data set was 2 seconds long.

   The data was processed using a simple method to yield updated signal deformation parameters [9]. Pseudo-range biases and tracking errors were obtained after accounting for temporal bias variations [10] using WAAS-GEO satellites as calibration sources.

   This approach provides very effective multipath mitigation. However, any time varying errors with non-zero biases between data sets would have to be measured using separate calibration sources, which could introduce additional errors into the measurements.

- Lower gain, simultaneous, long continuous data sets:
A rooftop survey-grade antenna was connected to specially modified aviation-grade receivers which could provide correlator outputs at different spacings (0.05, 0.1, 0.15 and 0.2 chips). Using the difference of these outputs (referenced to 0.1 chips), the signal deformation biases were obtained for all the satellites.

   The all-in-view nature of this approach provided observability and thus the ability to remove non-signal deformation-type, slow, common-mode time-varying biases. However, the limited multipath-rejection capability of the antenna allowed multipath to obscure the signal deformation errors. The results are summarized in Table 1.
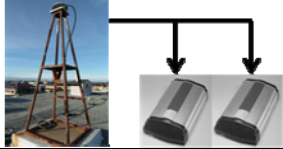
SRI Dish; Post-process	Rooftop Antenna; Modified Receiver
(+) High gain (low noise) (–) Short data set (2 sec)	(+) All-in-view; long continuous data set (–) Multipath rejection insufficient
Time-varying noise sources problematic	Signal deformation hidden by other noise (typically multipath)

Table 1. *Summary of the advantages and disadvantages of each approach to measure signal deformation.*

Thus, a new method was sought to combine the advantages of both previous approaches while mitigating their individual disadvantages, with the goal of observing and measuring signal deformation accurately and clearly.

In practice, it was not possible to accomplish this objective with a single approach. Instead, a combined approach was used:

- 1.8m mini dish antenna to collect data sets sequentially for each satellite for the entire time the satellite is in view.

  This would provide easily accessible, low-noise, low multipath measurements.

- All-in-view simultaneous, continuous data sets

  This would serve as a useful verification that there were no slow time-varying biases in the different data sets from the mini dish antenna.

The rest of this paper focuses on this combined approach – the measurement setup, results, comparison with past results and the impact on the user.

MEASUREMENT SETUP – MULTIPATH-LIMITING ANTENNA

5 different antenna types were used to collect raw pseudorange measurements. These are summarized in Table 2.

Antenna	Description
	Survey-grade geodetic antennas by 2 different manufacturers) (All-in-view)
	Choke Ring Multipath Limiting Antenna (All-in-view)
	Helibowl Multipath Limiting Antenna (All-in-view)
	Controlled Reception-Pattern Array (CRPA) Antenna [4] (All-in-view)
	1.8m Mini-Dish Antenna (Sequential)

Table 2. *Different antennas used for measurement collection.*

The first 4 antennas were all-in-view, with varying degrees of multipath attenuation. The last antenna provided effective multipath attenuation, but was also highly-directional with a narrow beamwidth and only able to receive data from one or at most two satellites at a time.

MEASUREMENT SETUP – MULTIPATH-LIMITING ENVIRONMENT

The measurements were collected in 3 different locations. These are summarized in Table 3.

Environment	Description
	Regular rooftop (baseline)
	Roble Field (low multipath)
	Lake Lagunita (dry lake bed) (low multipath)

Table 3. *Different locations for measurement data collection. Roble Field and Lake Lagunita had less reflective obstacles and thus were environments with less multipath.*

MEASUREMENT SETUP – RECEIVER

A COTS USRP receiver [**3**, **5**, **12**] was specially configured to provide 5 tracking loops, each set at a different correlator spacing {0.1, 0.2, 0.3, 0.4, 1.0 chips}, for each channel. This capability was essential for measuring the effects of nominal signal deformation. The multiple tracking loops and channels were all executing as parallel processes in a single COTS PC (Fig **5**). The tracking loops were all synchronized to a common clock, thus providing pseudoranges with common clock errors which were easily removed via single-differencing.
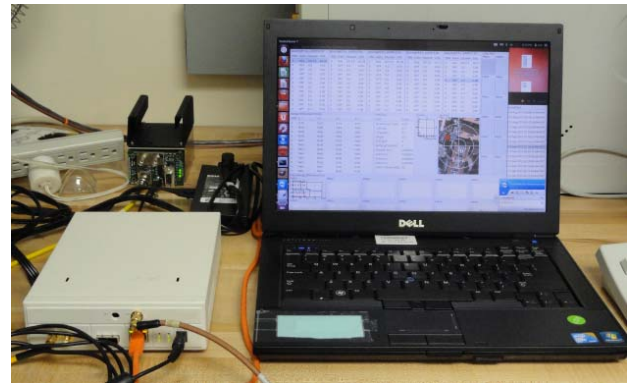

Figure 5. *COTS USRP GPS receiver on a single PC, providing pseudorange outputs at 5 different correlator spacings, all synchronized to a common clock. This is equivalent to the output of 5 GPS receivers executing simultaneously in real-time.*

PROCESSING OF RAW PSEUDORANGES FROM TRACKING LOOPS SET AT DIFFERENT CORRELATOR SPACINGS

As described in equation (2), single-differenced differential pseudoranges were formed to remove all sources of common-mode error except for the differential multipath, signal deformation and white noise errors (Figure 6). (Using a synchronized common clock allowed the differential user clock error to be removed via single-difference).
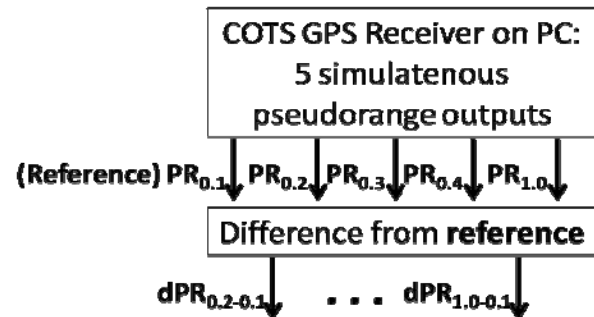

Figure 6. *Graphical illustration of the processing of the 5 simultaneous pseudorange outputs from the COTS GPS receiver to yield differential single-differenced pseudoranges.*

The narrowest correlator spacing (0.1 chip) was used as the reference for all the other spacings. A set of 4 single-differenced pseudoranges were formed by differencing the pseudorange at 0.1 chips from the pseudoranges at 0.2, 0.3, 0.4 and 1 chip correlator spacings. This was computed for each time epoch and each satellite in view.

The set of 4 single-differenced pseudoranges were each separately put through a 100-sec averaging filter to remove the white noise as mentioned in equation (2).

These final single-differenced, filtered pseudorange observables contained both constant nominal signal deformation biases, as well as time-varying multipath, which potentially had non-zero means. The computed standard deviations of the signals provided an indication of the residual amount of multipath. Lower standard deviations relative to the computed signal deformation biases implied higher confidence in the measured signal deformation biases.

Finally, once biases for individual satellites had been determined, the average bias across all satellites was computed and removed from individual satellite biases. This was performed to remove common mode effects from the filter and satellite dish which would not affect navigation solutions.

RESULTS – PRESENCE OF MULTIPATH AND MULTI-APPROACH VERIFICATION

Table 4 summarizes the effectiveness (as indicated by standard deviation) of the different approaches to mitigate multipath. The table shows that as the user correlator spacing increases, multipath errors increase, leading to increased standard deviations for all antenna types.

Configuration		User Correlator Spacing (Chips) (Ref: 0.1)			
		0.2	0.3	0.4	1.0
Environment	*Antenna*	*Average Standard Deviation (m)*			
Rooftop	Geodetic Survey-Grade	0.11	0.2	0.26	0.39
Rooftop	Choke-Ring/ Helibowl	0.08	0.13	0.18	0.31
*Roble Field/ Lake Lagunita	Helibowl	0.04	0.08	0.11	0.18
Rooftop/ Lake Lagunita	CRPA	Not suitable			
Rooftop	1.8m Mini-Antenna Dish	0.02	0.04	0.05	0.09

Note: *Roble Field/ Lake Lagunita: Due to practical limitations in data collection, results were based only on 1-4 hours of collected data.
Table 4. *Summary of standard deviations (indicative of multipath) for the different environments and antennas.*

Past data [**10**] indicated that the levels of signal deformation was ±0.1 to ±0.2m for the {0.2 – 0.1 chip} configuration, and up to ±0.4m for the {1.0 – 0.1 chip} configuration. To measure nominal signal deformation accurately, the multipath in the measurements was required to be a fraction of these values.

As table 4 showed, the rooftop geodetic survey-grade antennas contained residual multipath on the same order as the signal deformation biases. The rooftop multipath-limiting antennas (choke-ring/helibowl) provided better multipath attenuation, giving greater confidence in the signal deformation bias measurements. Making use of low-multipath environments decreased the residual multipath noise further; however, this was impractical for long-term data collection as it involved transporting cumbersome lab equipment to remote locations with inadequate power and security.

The Controlled Pattern Reception Array (CRPA) Antenna [**4**], in both the rooftop and lower-multipath environments, was effective in reducing strong, directed multipath and interference and maintaining high levels of signal power. Unfortunately, it was found unsuitable for measuring signal deformation. This is because each individual antenna formed a replica with a slightly different, non-constant delay in time. Coupled with the phase uncertainties associated with each COTS antenna, the overall uncertainties were larger than and obscured the signal deformation biases.

The sequential rooftop 1.8 mini-antenna dish was not only a more practical means of data collection, it was also able to produce measurements with sufficiently low residual multipath to provide good confidence in the measurements. What remained was to ensure there were no slowly-varying, unobservable biases or drifts between the sequential measurements. This was verified by comparing the all-in-view measured biases with the sequentially-measured biases and checking for consistency between the different approaches.

The following figures show the distribution of the signal deformation biases for individual satellites, together with the standard deviations associated with each approach. **These figures focus on a user correlator spacing of 0.2 chips only. Figures for user correlator spacing of 1.0 chips are shown in the next section).** For this measurement configuration, nominal signal deformation biases were the smallest; however multipath was also the smallest, thus providing more confidence in the accuracy of the measurements. All the results are for satellites above a 30° elevation angle mask.

Figure 7 shows results for the rooftop geodetic survey antennas. The individual distribution shows many individual satellite biases that are on the order of, or smaller than, the standard deviation of 0.11m. Solely based on these results, we cannot determine if the biases were from satellite signal deformation, or were corrupted by biased multipath.
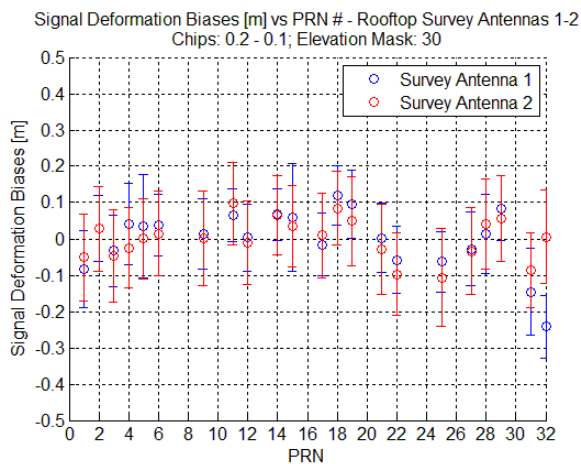
Figure 7. *Signal deformation biases and standard deviations (uncertainty) distributions for individual satellites for all-in-view geodetic survey antennas on rooftop. Reference receiver: 0.1 chips; User receiver: 0.2 chips. Elevation angle mask = 30°. Average standard deviation ≈ 0.11m.*

Figure 8 shows results for the rooftop multipath-limiting antennas (choke-ring and helibowl). Notably, the standard deviations (error bars) have reduced in magnitude, to an average value of 0.08m. However, a good many of the signal deformation biases are still smaller in magnitude than the average standard deviation.
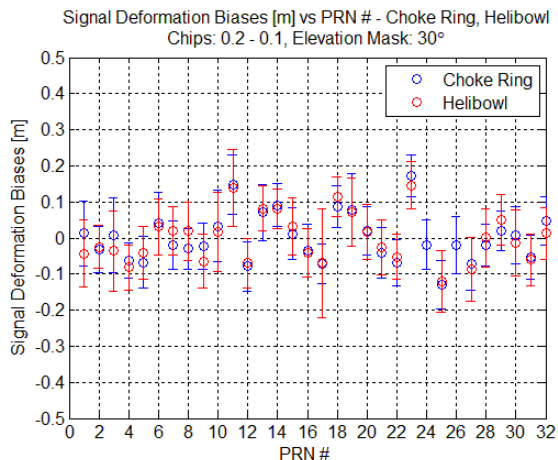

Figure 8. *Signal deformation biases and standard deviations (uncertainty) distributions for individual satellites for all-in-view multipath-limiting antennas on rooftop. Reference receiver: 0.1 chips; User receiver: 0.2 chips. Elevation angle mask = 30°. Average standard deviation ≈ 0.08m.*

Figure 9 shows results for the sequential 1.8m mini-antenna dish approach. The standard deviations are noticeably smaller in magnitude than the majority of the satellite signal deformation biases. Thus this approach seems to provide the best multipath rejection, and appears

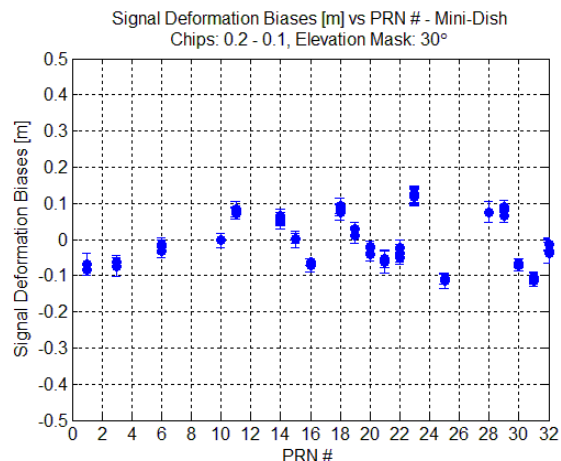to accurately measure even the smallest signal deformation biases.

Figure 9. *Signal deformation biases and standard deviations (uncertainty) distributions for individual satellites for sequential 1.8m mini-dish antenna on rooftop. Reference receiver: 0.1 chips; User receiver: 0.2 chips. Elevation angle mask = 30°. Average standard deviation ≈ 0.02m, sufficient to measure even the smallest signal deformations.*

The following figure, Figure 10, shows the remarkable consistency between the all-in-view and sequential approaches. This confirms that any possible drifts between the individual data sets in the sequential mini-dish approach are small. Any discrepancies are well within the uncertainties (standard deviations) due to multipath. **This figure confirms that nominal signal deformation biases are small but present in the satellite signals, and can be measured at the output of regular GPS receivers**. Other research findings [**1, 6, 7, 8**] confirm that non-zero nominal signal deformation biases are present in satellite signals.
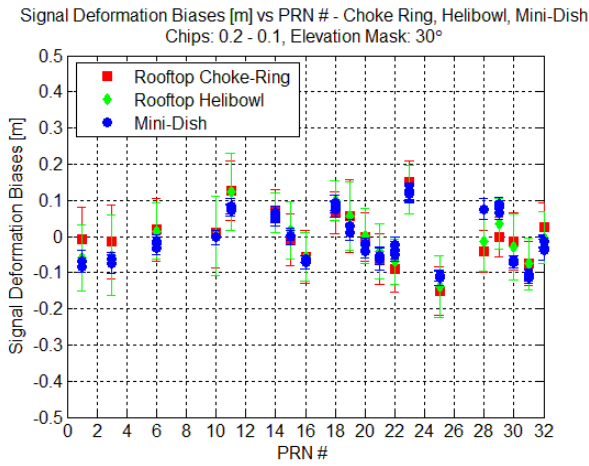
Figure 10. *Signal deformation biases and standard deviations (uncertainty) distributions for individual satellites for <u>sequential</u> 1.8m mini-dish antenna and <u>all-in-view</u> multipath-limiting antennas on rooftop. Reference receiver: 0.1 chips; User receiver: 0.2 chips. Elevation angle mask = 30°. The biases from the two different approaches show remarkable consistency with each other.*

WORST CASE POSITION ERROR

Previous results [**10**] showed that the configuration of reference receiver correlator spacing of 0.1 chips and a user receiver correlator spacing of 1.0 chips should result in the largest signal deformation biases. These would have the worst case impact on position error. The distribution of these biases is shown in Figure 11, for both sequential mini-dish antenna and all-in-view antennas. As can be seen, the signal deformation biases are indeed larger (≈ **0.3m**) compared to previous case (≈ **0.15m**) for user correlator spacing of 0.2 chips. However, there is also less of a match between the sequential and all-in-view antennas. This can be attributed to increased multipath, which can be seen from the increased standard deviation error bars.
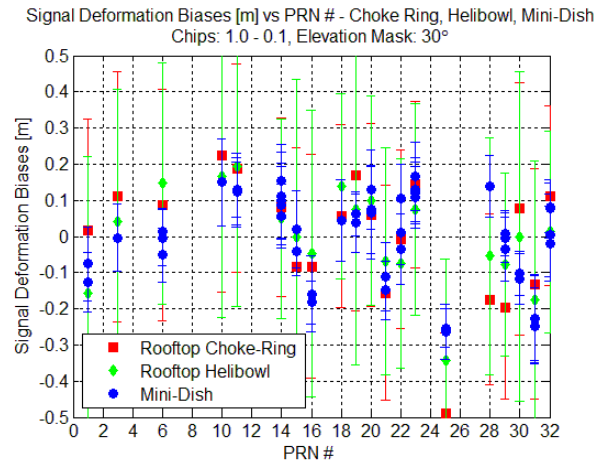

Figure 11. *Signal deformation biases and standard deviations (uncertainty) distributions for individual satellites for <u>sequential</u> 1.8m mini-dish antenna and <u>all-in-view</u> multipath-limiting antennas on rooftop. <u>Reference receiver: 0.1 chips; User receiver: 1.0 chips</u>. Elevation angle mask = 30°. Consistency between the sequential and all-in-view approaches is not as high as before, due to increased multipath.*

The magnitudes of measured signal deformation biases for user correlator spacings of both 0.2 chips and 1.0 chips match those from previous results [**10**]. In cases of dual-frequency and broken geometry, these biases can cause worst case vertical position errors as shown in Table 5 [**11**]. A user receiver with a narrow correlator spacing of 0.2 chips could experience worst case vertical position errors of **1.3-1.9m**; the same user receiver with a wider correlator spacing of 1.0 chips could experience worst case vertical position errors of **2.7-4m**. These vertical position errors are significant, showing the importance of error bounds for nominal signal deformation [**11**] and of limiting user correlator spacings to at most 0.2 chips.

Satellite Configuration	DUAL FREQUENCY (0.2 - 0.1 Chips)			DUAL FREQUENCY (1.0 - 0.1 Chips)		
		Position Errors [m]			Position Errors [m]	
	Avail	99%	Max	Avail	99%	Max
All-in-view	100.0%	0.45	0.51	100.0%	0.44	0.56
N - 1	100.0%	0.49	1.27	100.0%	0.63	2.70
N - 2	99.9%	0.57	1.50	99.9%	0.80	3.09
N - 3	99.2%	0.66	1.56	99.3%	0.97	3.40
N - 4	97.3%	0.73	1.68	97.4%	1.18	3.81
N - 5	91.9%	0.83	1.89	92.2%	1.40	3.86

Table 5. *Worst case dual frequency position errors for given signal deformation biases for user correlator spacings of 0.2 chips and 1.0 chips. The different rows show the results for different cases of broken geometries.*

CONCLUSION

A combined approach of two methods was used to demonstrate nominal signal deformation errors in the pseudorange domain, at the output of an actual hardware receiver. The two methods complement each other, providing accurate low multipath measurements with the ability to observe and remove (if needed) common-mode time variations. Both methods yield results which are mutually consistent and show signal deformation biases of ±0.15m for user correlator spacing of 0.2 chips and ±0.3m for user correlator spacing of 1.0 chips. For dual frequency SBAS, these could cause worst case vertical position errors of 1.3-4m. These results highlight the advantages of narrow user correlator spacings and the need for the error bounds to take nominal signal deformation errors into account.

ACKNOWLEDGEMENT

REFERENCES

[1] Brenner, M., Kline, P., Reuter, R., "Performance of a Prototype Local Area Augmentation System (LAAS) Ground Installation", Proceedings of ION GPS 2002, Portland, OR, Sep 2002

[2] Blanch, J., Walter, T., Enge, P., "A Clock and Ephemeris Algorithm for Dual Frequency SBAS", Proceedings of the 24th International Technical Meeting of The Satellite Division of the Institute of Navigation (ION GNSS 2011), Portland, September 2011

[3] Chen, Y-H., Juang, J-C., et. al, "Real-Time Software Receiver for GPS Controlled Reception Pattern Array Processing", Proceedings of the 23rd International Technical Meeting of The Satellite Division of the Institute of Navigation (ION GNSS 2010)

[4] Chen, Y-H., "A Study of Geometry and Commercial Off-The-Shelf (COTS) Antennas for Controlled Reception Pattern Antenna (CRPA) Arrays", Proceedings of the 25th International Technical Meeting of The Satellite Division of the Institute of Navigation (ION GNSS 2012), Nashville, September 2012

[5] Chen, Y-H., Juang, J-C., et al, "Design and Implementation of Real-time a Software Radio for Anti-Interference GPS/WAAS Sensors", Accepted for Publication Sensors 2012

[6] Gunawardeena, S., van Grass, F., "Analysis of GPS Pseudorange Natural Biases using a Software Receiver", Proceedings of the 25th International Technical Meeting of The Satellite Division of the Institute of Navigation (ION GNSS 2012), Nashville, September 2012

[7] Phelts, R.E., "Nominal Signal Deformations: Limits on GPS Range Accuracy", The 2004 International Symposium on GPS/GNSS, Sydney, Australia, December 2004

[8] Phelts, R. E., Walter, T., Enge, P., "Characterizing Nominal Analog Signal Deformations on GNSS Signals", Proceedings of the 22nd International Technical Meeting of The Satellite Division of the Institute of Navigation (ION GNSS 2009), Savannah, GA, September 2009

[9] Wong, G., Phelts, R.E., Walter, T., Enge, P., "Characterization of Signal Deformations for GPS and WAAS Satellites", Proceedings of the 23rd International Technical Meeting of The Satellite Division of the Institute of Navigation (ION GNSS 2010), Portland, September 2010

[10] Wong, G., Phelts, R.E., Walter, T., Enge, P., "Alternative Characterization of Analog Signal Deformation for GNSS-GPS Satellites", Proceedings of the 2011 International Technical Meeting of The Institute of Navigation, San Diego, January 2011

[11] Wong, G., Phelts, R.E., Walter, T., Enge, P., "Bounding Errors Caused by Nominal GNSS Signal Deformations", Proceedings of the 24th International Technical Meeting of The Satellite Division of the Institute of Navigation (ION GNSS 2011), Portland, September 2011

[12] Universal Software Radio Peripheral. Retrieved Sept 29, 2012, from http://en.wikipedia.org/wiki/Universal_Software_Radio_Peripheral